Manuscript Details

Manuscript number DSR2_2018_93

Title Calcareous nannofossil palaeoenvironmental reconstruction and preservation during sapropel S1 at the Eratosthenes Seamount (Eastern Mediterranean)

Abstract

The most recent carbon-enriched layer (sapropel S1) deposited at the Eratosthenes Seamount has unique features, such as an early lithological interruption, fine light silt laminae and an exceptional vertical extent that is over 25 cm thick. Here we investigate calcareous nannofossil assemblages to reconstruct very high-resolution palaeoenvironmental and palaeoceanographic variations recorded before, during and after the perturbation episode that involved the eastern Mediterranean Sea, due to the massive freshwater discharge via Nile River. Our results show that the deep chlorophyll maximum development, observed in all micropalaeontological groups from previous studies, is a gradual process that started well before the base of sapropel S1. A high-frequency variability in the nutricline depth is evident at millennial- and/or centennial-scale throughout the sapropel deposition time interval. Also we highlight the poor-preservation of delicate tiny holococcolith crystals while anoxia was occurring at the seafloor and we suggest that such a phenomenon may be used to mark the original thickness of sapropel deposition where oxygen re-ventilation fronts were developed. Finally, calcareous nannofossil reworking peaks shed light on the nature of fine silt laminae within the sapropel S1 at the Eratosthenes Seamount, which may be ascribed to fine sediment plumes from the Nile River deposited during exceptional runoff events.

Submission Files Included in this PDF

File Name [File Type]

Incarbona and Di Stefano (968)DSR.docx [Manuscript File]

Fig. 1 (DSRII).jpg [Figure]

Fig. 2 (DSRII).jpg [Figure]

Fig. 3 (DSRII).jpg [Figure]

Fig. 4 (DSRII).jpg [Figure]

Fig. 5 (DSRII).jpg [Figure]

Fig. 6 (DSRII).jpg [Figure]

To view all the submission files, including those not included in the PDF, click on the manuscript title on your EVISE Homepage, then click 'Download zip file'.

Research Data Related to this Submission

There are no linked research data sets for this submission. The following reason is given:
Data will be made available on request

Calcareous nannofossil palaeoenvironmental reconstruction and preservation during sapropel S1 at the Eratosthenes Seamount (Eastern Mediterranean)

Alessandro Incarbona*, Enrico Di Stefano

Università degli Studi di Palermo, Dipartimento di Scienze della Terra e del Mare, Via Archirafi 20-22, 90134 Palermo, Italy

*Corresponding author: Alessandro Incarbona, e-mail: alessandro.incarbona@unipa.it; Telephone: +3909123864648

Abstract

The most recent carbon-enriched layer (sapropel S1) deposited at the Eratosthenes Seamount has unique features, such as an early lithological interruption, fine light silt laminae and an exceptional vertical extent that is over 25 cm thick. Here we investigate calcareous nannofossil assemblages to reconstruct very high-resolution palaeoenvironmental and palaeoceanographic variations recorded before, during and after the perturbation episode that involved the eastern Mediterranean Sea, due to the massive freshwater discharge via Nile River. Our results show that the deep chlorophyll maximum development, observed in all micropalaeontological groups from previous studies, is a gradual process that started well before the base of sapropel S1. A high-frequency variability in the nutricline depth is evident at millennial- and/or centennial-scale throughout the sapropel deposition time interval. Also we highlight the poor-preservation of delicate tiny holococcolith crystals while anoxia was occurring at the seafloor and we suggest that such a phenomenon may be used to mark the original thickness of sapropel deposition where oxygen re-ventilation fronts were developed. Finally, calcareous nannofossil reworking peaks shed light on the nature of fine silt laminae within the sapropel S1 at the Eratosthenes Seamount, which may be ascribed to fine sediment plumes from the Nile River deposited during exceptional runoff events.

Keywords

Florisphaera profunda; Holococcolith; Nutricline depth; Seafloor preservation; African Monsoon

1 – Introduction

Eastern Mediterranean organic carbon-enriched layers (sapropels) are associated to precession minima (Hilgen, 1991; Lourens et al., 1997) that enhanced monsoon freshwater discharge via Nile

River (Hennekam et al., 2015; Marino et al., 2009; Rohling et al., 2002; Rossignol-Strick et al., 1982; Weldeab et al., 2014). These events led to a huge perturbations in the eastern Mediterranean circulation and in the whole Mediterranean conveyor belt. The hydrological deficit that drives the Mediterranean antiestuarine circulation pattern was never balanced, as demonstrated by the continuos deep water outflow in the Gulf of Cadiz and in the Iberian Margin (Bahr et al., 2015; Schönfeld and Zahn, 2000; Voelker et al., 2006; Zahn et al., 1987). The massive freshwater discharge caused a significant buoyancy gain in upper part of the water column, strongly inhibiting Adriatic and Aegean Sea deep water formation that failed to bring oxygen to the deep seafloor (De Lange et al., 2008; Rohling et al., 2015). These processes have definitively left a mark on ecosystems that are identified on fossil micro-organisms. Deep benthic life became extinct, although ~~some~~ exceptions exist due to local settings and glacial sapropels (Jorissen, 1999; Rohling et al., 2015; Schmiedl et al., 2003). The nutricline, that today is several hundred of metres depth, raised well within the lower photic zone. A distinct deep chlorophyll maximum (DCM) has been identified in all main phytoplankton groups (Castradori, 1993; Kemp et al., 1999; Meier, 2004) and even in planktonic foraminifera grazers (Rohling and Gieskes, 1989).

The most recent sapropel, the so-called sapropel S1, deposited below 1800 m depth in the open eastern Mediterranean, between 10.8 and 6.1 kiloyears ago (ka) (De Lange et al., 2008; Grant et al., 2016). It is the most studied sapropel layer because of the ease of recovery (just a few tens of centimetres below the seafloor) and the short time elapsed that allows an excellent chronological constraint and a realistic comparison with different paleoceanographic and paleoclimatic proxies. A distinct sapropel interruption, between 8.5 and 7.8 ka, marks a return of significant deep water oxygenation in the Aegean and Adriatic Seas (Casford et al., 2003; Rohling et al., 2015).

The sapropel S1 layer recovered during the Ocean Drilling Program (ODP) Leg 160, at the Eratosthenes Seamount setting (Site 968) has characteristics which are completely unique. The site is under direct influence of the Nile Delta Cone, at a depth which is close to permanent anoxia (~ 1900 m). Sapropel S1 consists of one of the largest thicknesses so far recovered and thus has the potentiality for high-resolution investigation. It is characterized by millimetre laminated mud interbeds and distinctive colour changes and an is interrupted by a thin clay layer near the base (Emeis et al., 1996). Here we present the study of coccoliths carried out every 1-cm of sediment, below, across and above sapropel S1. The aim of the study is to assess the palaeoenvironmental reconstruction of the photic zone during this crucial interval and to verify whether the unique lithological features of sapropel S1 at Site 968 match with environmental and preservation variations in calcareous phytoplankton assemblages.

2 - Material and Methods

2.1 - Sediment cores

ODP Hole 968C (34°19.976'N, 32°45.211'E, 1964.1 m water depth) is located at the base of the northern slope of the Eratosthenes Seamount, a structure that emerges from the Nile Delta Cone (Fig. 1). Lithology is dominated by calcareous gray and brown nannofossil clay and clayey nannofossil ooze (Emeis et al., 1996). No ash layers occur within the studied interval (Emeis et al., 1996). Sapropel S1 is about 25 cm thick (Fig. 2) and has an organic carbon content of 2% (Emeis et al., 1996). It is interrupted by a 0.5-cm thick clay near the base and is overlain by a distinctive Mn-rich zone. Many millimetre- and sub-millimetre-scale laminae, that consist of clay and pyrite, punctuate the sapropel layer.

2.2 - Coccolith data

Coccolith analysis at ODP Site 968 was carried out at 1 cm resolution, between 33 and 112 cm composite depth (cmcd), for a total of 79 samples. The coccolith analysis was carried out by observation with a polarized microscope at about 1000 X magnification. Rippled smear slides were prepared following the standard procedure (Bown and Young, 1998). A mean of 500 specimens within the entire assemblage was identified following the taxonomic concepts on living coccolithophores of Young et al. (2003) and Jordan et al. (2004). Taxa were grouped in 'placoliths', 'miscellaneous group', 'upper photic zone (UPZ) group', 'lower photic zone (LPZ) group' and 'holococcoliths'(Di Stefano and Incarbona, 2004; Incarbona et al., 2010b). Placoliths include small placoliths, small *Gephyrocapsa*, *Gephyrocapsa muellerae* and *Gephyrocapsa oceanica*. Miscellaneous group includes *Helicosphaera* spp., *Coccolithus pelagicus*, *Syracosphaera histrica*, *Pontosphaera* spp., *Calcidiscus leptoporus*, *Pleurochrysis* spp., *Braarudosphaera* spp., *Oolithotus fragilis*, *Calciosolenia* spp. and specimens of all the other species. UPZ group includes *Syracosphaera pulchra*, *Umbellosphaera* spp., *Discosphaera tubifera*, *Rhabdosphaera* spp., *Umbilicosphaera* spp. and *Ceratolithus* spp. LPZ group includes *F. profunda* and a negligible number of *Gladiolithus flabellatus* specimens. Holococcoliths include all the coccoliths produced during the holococcolithophore life stage.

The CEX dissolution Index was performed following Dittert et al. (1999): Number of specimens of (*E. huxleyi*) / Number of specimens of (*E. huxleyi* + *C. leptoporus*). Values close to 1 suggest little or no dissolution effects on coccolith assemblages. N ratio follows Flores et al. (2000) and is expressed by: (small *Noelaerhabdaceae*) / (small *Noelaerhabdaceae* + *F. profunda*). Values close to 1 and close to 0 respectively indicate a shallow and a deep nutricline within the photic zone.

2.3 – Species and groups ecological preference

Placoliths are r-strategist taxa that bloom after nutrient fertilization (Flores et al., 2000; Incarbona et al., 2010b; Young, 1994). Among them, *E. huxleyi* is a cosmopolitan and opportunistic taxon that dominates today's ocean assemblages (Young, 1994). In the Mediterranean Sea, this taxon blooms preferentially during winter and spring, after vertical convection that fuels nutrients into the photic zone (Di Stefano et al., 2011; Knappertsbusch, 1993). LPZ taxa and the species *F. profunda* peak in response to nutricline deepening within the photic zone (Beaufort et al., 1997; McIntyre and Molfino, 1996; Molfino and McIntyre, 1990a, 1990b). UPZ and Miscellaneous taxa are K-strategist and weakly K-strategist organisms, respectively (Incarbona et al., 2010b; Young, 1994). Holococcoliths are produced by coccolithophores during their haploid life phase. Although belonging to different species, they behave as a homogeneous group (Oviedo et al., 2015), preferring warm and oligotrophic surface waters (Kleijne, 1991; Knappertsbusch, 1993; Oviedo et al., 2015).

2.4 – Chronology

The chronology follows Konijnendijk et al. (2014) who carried out a precise correlation between the Ti/Al record at ODP 967/968 Site and the radiometrically-dated $\delta^{18}O$ record of speleothems from Hulu and Sanbao caves (Wang et al., 2008). This choice relies upon the fact that the Ti/Al ratio reflects Nile River suspended matter and windblown dust (Lourens et al., 2001; Wehausen and Brumsack, 2000). Titanium is a heavy element, preferentially deposited close to the river mouth. River-derived sediments are essentially Titanium depleted and this element is predominantly brought by aeolian inputs during poor precipitation and vegetation cover in North Africa. The average sedimentation rate for the whole studied interval is 7.8 cm/kyr, significantly higher than most of eastern Mediterranean records, and the sampling resolution is 128 years. Within the sapropel layer, the average sedimentation rate is 5.2 cm/kyr and the sampling resolution is 192 years.

3 – Study area

Modified Atlantic Water (MAW) enters the eastern Mediterranean Sea by the Mid-Mediterranean Jet that flows in the central Levantine Basin up to Cyprus and the Eratosthenes Seamount. A quasi-permanent anticyclonic summer circulation, called Shikmona Gyre, is located in the Eratosthenes Seamount area (Malanotte-Rizzoli et al., 2014; Pinardi and Masetti, 2000; POEM group, 1992). Intermediate water forms in winter as a process of surface cooling and evaporation of salty-enriched water masses. The formation area of intermediate waters is close to the Eratosthenes Seamount (POEM group, 1992). Eastern Mediterranean dense water forms in the Adriatic and Aegean Sea

(Fig. 1) and fills the Ionian and Levantine Sea bottom. Deep water formation in the Adriatic and Aegean Sea is promoted by winter heat flux loss, when Bora and Vardar intensely blow. The heat loss in these two regions is significantly influenced by variations in East Atlantic and East Atlantic/Western Russian atmospheric patterns (Josey et al., 2011).

The eastern Mediterranean Sea is severely oligotrophic. Primary productivity reflects the nutrient depletion (Krom et al., 2010, 1991) and is higher in winter, and severely lower in summer, due to the deepening of thermocline and nutricline (Allen et al., 2002; D'Ortenzio and Ribera d'Alcalà, 2009; Klein and Coste, 1984).

The transition between the subtropical high-pressure belt over North Africa and westerlies over central and western Europe controls seasonal variations in the Mediterranean/Europe region. The northward shift of this transition in summer causes drought over most of the Mediterranean. In winter, the southward displacement of the transition allows the penetration of westerlies and Atlantic depressions (Rohling et al., 2015). In winter and spring, polar air masses are channelled through valleys and flows in the Adriatic and Aegean Seas, where they produce intense surface cooling and evaporation and contribute to deep water formation (Poulos et al., 1997; Rohling et al., 2015).

4 – Results

The dominant taxa in the investigated record are *E. huxleyi* (16.6-75.0 %, 49.5 % on average) and *F. profunda* (8.9-78.2 %, 37.8 % on average) (Fig. 3). *Florisphaera profunda* is the dominant species during sapropel S1, but differently from many previous reports (Castradori, 1993; Incarbona et al., 2011; Negri et al., 1999) it increases gradually since the last deglaciation. Holococcoliths are abundant below and above sapropel S1 (0.0-11.7 %, 4.6 % on average) (Fig. 3) and are mainly belonging to *S. pulchra* HOL *oblonga* (*Calyptrosphaera oblonga*), as already observed in late Quaternary Mediterranean sediments (Crudeli et al., 2006; ~~A.~~ Di Stefano et al., 2015). All the other taxa belonging to placolith (small *Gephyrocapsa*), UPZ (*S. pulchra*, *Umbellosphaera* spp., *D. tubifera* and *U. sibogae*) and Miscellaneous groups (*S. histrica*) occur with percentage values lower than 5 % (figs 3 and 4). *Gephyrocapsa muellerae* and *G. oceanica* that are abundant in the central and western Mediterranean record, respectively in the deglaciation and in the early Holocene (Ausín et al., 2015; Bazzicalupo et al., 2018; Buccheri et al., 2002; Cacho et al., 2001; Colmenero-Hidalgo et al., 2004; ~~Agata~~ Di Stefano et al., 2015; Di Stefano and Incarbona, 2004; Flores et al., 1997; Incarbona et al., 2009), are substantially absent (not shown in figures). Reworked specimens, pertinent to extinct Mesozoic and Cenozoic taxa, ranges between 0.0 and 7.8% (1.6 % on average), with values that are generally well below 2.0 % and a few distinctive peaks (Fig. 3). Placolith (16.7-

78.7 %, 51.1 % on average) and LPZ (8.9-78.6 %, 38.0 % on average) groups exactly mirror the abundance patterns of respectively *E. huxleyi* and *F. profunda* (Fig. 5). UPZ (2.0-9.9 %, 5.0 % on average) and Miscellaneous (0.0-4.1 %, 1.4 % on average) do not show any distinctive abundance peak throughout the sequence (Fig. 5).

5 – Discussion

5.1 – Palaeoenvironmental reconstruction

The most significant palaeoenvironmental signal recorded within sapropel S1 at the Eratosthenes Seamount location is the establishment of a deep nutricline in the lower photic zone and the development of a DCM. This phenomenon, indicated by the abundance increase of *F. profunda* (Figs. 3 and 5), has exhaustively been discussed in different papers (Castradori, 1993; Grelaud et al., 2012; Incarbona et al., 2011; Negri et al., 1999; Triantaphyllou et al., 2009b, 2010; Triantaphyllou, 2014) and is also visible in planktonic foraminifera, diatom and dinoflagellate palaeoenvironmental reconstructions (Kemp et al., 1999; Meier, 2004; Rohling and Gieskes, 1989). In Figure 6 we highlight the DCM development by the N ratio, independent from the closed-sum effect and previously applied to different oceanic settings (Bazzicalupo et al., 2018; Flores et al., 2000; Leonhardt et al., 2015; López-Otálvaro et al., 2009), that testifies to the nutricline position deepening. The N ratio pattern shows gradual variations that closely mirror the precession Index (Rossignol-Strick, 1985; Rossignol-Strick et al., 1982) calculated as the difference between the Tropic of Cancer and the Equator insolation. This behaviour is different from previous studies that report an abrupt nutricline shift just in coincidence of the sapropel base (Castradori, 1993; Incarbona et al., 2011; Negri et al., 1999; Triantaphyllou et al., 2009a). The only similar record in literature is possibly from core BC06 recovered in the Ionian Sea (Negri and Giunta, 2001), even though a chronology for this core is lacking and thus we cannot precisely correlate the *F. profunda* abundance increase that at 968 Site starts since the Younger Dryas.

The sequence of East African monsoon activity and the subsequent Nile River discharge is well-summarized by Ba/Ca data collected in the delta sediments, that define monsoon intensification since the Holocene base and a distinctive maximum flooding at 10.0 ka (Fig. 6C) (Hennekam et al., 2015; Rohling et al., 2015; Weldeab et al., 2014). The maximum Nile River discharge at 10.0 ka is a distinctive mark impressed by the East Africa monsoon on eastern Mediterranean sediments, with respect to Asian monsoon activity that seems to be more regularly punctuated by Dansgaard-Oeschger oscillations (Fig. 6D) (Cheng et al., 2016). This means that the gradual nutricline deepening at the Eratosthenes Seamount site may be due to climatic forcing different from, or not only due to, freshwater discharge into the eastern Mediterranean Sea. Variations in insolation (Fig.

6B) are a primary factor for nutricline shift within the photic zone in many ocean settings (Beaufort, 1997; Beaufort et al., 2001; Molfino and McIntyre, 1990a) and in the eastern Mediterranean may have fostered the deepening of a seasonal thermocline since the deglaciation. In fact, deep-water ventilation data and an ocean-biogeochemical model have suggested that sapropel S1 deep-water anoxia would have required deep-water stagnation since the latest glacial period, possibly due to the long-term insolation-driven African runoff, warming and sea-level rise (Grimm et al., 2015). Further high-resolution studies are needed to understand nutricline depth dynamics across the eastern Mediterranean Sea during sapropel S1 that may contain relevant information on climatic and oceanographic forcings.

Finally, the N ratio curve sheds light on high-frequency variability in the Eratosthenes Seamount upper water column, above about 10.0 ka (black arrows in Fig. 6). One of these episodes, characterized by nutricline shallowing, is clearly associated with the 8.2 ka event, that led to sapropel interruption in the Adriatic and Aegean Seas (Casford et al., 2003; Mercone et al., 2001; Rohling et al., 2015, 1997). The high-frequency variability is even more evident in the distribution patterns of placolith (or *E. huxleyi*) and LPZ (or *F. profunda*) groups (black arrows in Figs. 3 and 6), where it apparently covers the whole sapropel S1 extent. These oscillations are compatible with millennial-scale Bond cycles (Bond et al., 2001, 1997), that are well-known in the Holocene record of central and western Mediterranean sites (Frigola et al., 2007; Incarbona et al., 2008b). However, some of the cycles may have occurred with a shorter periodicity, perhaps similar to centennial-scale ventilation variability noted by (Jilbert et al., 2010). A more resolved age model, for instance based on radiocarbon datings, should be needed to carry out a careful spectral analysis. In any case our study highlights the occurrence of millennial- and/or centennial-scale environmental variability during the deposition of sapropel S1.

5.2 – Holococcolith preservation during S1

The holococcolith distribution pattern at Hole 968C is surprisingly similar to color lightness variations (Figs. 6E-F). Holococcoliths near disappear throughout the sapropel S1 layer, while sediment colour is dark. Poor preservation of holococcoliths in sapropel S1 was previously noted by Crudeli et al. (2006) and was explained by the fact that when dense water renewal on the sea bottom fails, tiny holococcolith crystals are dissolved during early diagenesis, possibly by aggressive pore water (Thomson et al., 2004). This process is compatible with maximum wetness in the wet/dry index (Fig. 6G) based on elemental proxies at the Eratosthenes Seamount (ODP Site 967) by Grant et al. (2017).

It is worth noting that holococcolith preservation seems to be very sensitive to seafloor redox conditions and record a short interval of enhanced preservation together with colour lightening, centred at about 8.2 ka, that may be correlated to monsoon activity weakening and the sapropel interruption in the Adriatic and Aegean Seas (Mercone et al., 2001; Rohling et al., 1997). We suggest that the potentiality of holococcolith preservation may identify the original extent of sapropel deposition even for post-depositional oxigenation, like actually done by Ba/Al excess curves (De Lange et al., 2008; Mercone et al., 2001; Rutten et al., 2000). Future attempts should be aimed at the reconstruction of holococcolith abundances in sapropels that have registered downward-moving oxidation fronts.

An in-depth examination of holococcolith and colour lightness signals reveals that holococcolith and colour lightness curves are slightly misaligned. The 2-3 cm bias cannot be explained by sampling inaccuracy. Also we have checked possible mistakes in the original dataset of colour lightness at Hole 968C, comparing it with data from Hole 968A and we can confirm its correctness. Since the holococcolith shifts precede those in the colour curve, we may hypothesize that holococcolith dissolution and preservation occur in a diagenetic environment, a few centimetres below the seafloor. Further research is needed to assess this point and verify the possible distortion of the holococcolith signal with respect to the rest of the nannofossil assemblage.

Holococcolith is a clear preservation signal impressed in the sedimentary record of the eastern Mediterranean Sea. The CEX index is usually employed to verify coccolith preservation, but it does not show any significant deviation from values very close to 1 (Fig. 6H). This suggests that the index is not suitable to ascertain coccolith preservation in the eastern Mediterranean Sea and/or that dissolution did not severely affect the rest of calcareous nannofossil assemblages.

5.3 – Coccolith reworking and Nile River sediment plumes

Coccolith reworking is a useful tool in palaeoenvironmental reconstruction to understand processes and interactions with land. Sea-level variations and the vertical shift of the erosion base, changes in the vegetation cover, river runoff and primary productivity dilution are common explanation for reworked variations (Incarbona et al., 2010a, 2009, 2008a). The coccolith reworking pattern shows several distinctive peaks (Fig. 6I) and most of them can be correlated with minima in the Ti/Al record (Fig. 6J) of the same ODP Site 968 (Konijnendijk et al., 2014). This suggests that an increased number of reworked specimens deposited in coincidence of intense episodes of Nile runoff (Lourens et al., 2001; Wehausen and Brumsack, 2000). This consideration is compatible with abundant Mesozoic taxa that outcrops along the Nile River catchment.

The occurrence of coccolith reworked specimens in the 968 record during the investigated record strongly supports the hypothesis that fine silt laminae within sapropel S1 is material deposited from Nile River plumes (Cita et al., 1984; Emeis et al., 1996). In fact, although beyond the aim of this paper, the observation of foraminifera assemblages does not reveal the occurrence of significant amount of dysoxic benthic specimens that mark re-ventilation episodes and may provide an alternative explanation for the lighter colour of these laminae.

6 – Conclusions

A total of 79 calcareous nannofossil samples from ODP Hole 968C, at the Eratosthenes Seamount setting, was investigated across sapropel S1, with an average sampling resolution of 128 years. The species *E. huxleyi* and *F. profunda* are overwhelmingly dominant and provide valuable evidence of nutricline depth variations. No significant variations are observed in taxa that thrive without a distinct depth preference (Miscellaneous group) or in K-strategist taxa (UPZ group).

As previously noted in different reports, a DCM marks the sapropel deposition time interval. However, at the Eratosthenes Seamount location it is evident that the DCM development is a gradual phenomenon started since the last deglaciation. The comparison with proxy data for Nile River runoff suggests that the freshwater discharge is possibly not the unique forcing of this process that may have been also driven by increasing insolation values.

Nutricline depth variations have been inferred on the basis of the N ratio (Flores et al., 2000), that exploits the abundance of dominant species and is irrespective of closed-sum effect. The distribution pattern of this ratio shows that nutricline depth changed with a high-frequency pace that may be due to millennial-scale Bond cycles (Bond et al., 1997, 2001) and/or to centennial-scale variability, previously noted in eastern Mediterranean seafloor ventilation (Jilbert et al., 2010).

The holococcolith distribution pattern follows sediment colour lightness variations. This relationship is interpreted as the result of holococcolith poor-preservation during sapropel S1 deposition. This phenomenon was previously noted by Crudeli et al. (2006) and we further stress that such a signal may be used as a sapropel original thickness marker after carbon matter burn-down. Future research should assess whether coccolith analysis is able to distinguish the original extent of oxidized sapropel layers and whether holococcolith dissolution and preservation occur in a diagenetic environment, a few centimetres below the seafloor.

Distinctive peaks of coccolith reworked specimens are correlated to minima in the Ti/Al record of Konijnendijk et al. (2014), suggesting that they are deposited in coincidence of intense Nile runoff episodes. This observation strongly supports the hypothesis that fine silt laminae within sapropel S1 is material deposited from Nile River plumes (Cita et al., 1984; Emeis et al., 1996).

Acnowledgment

This research was supported by Italian Ministry of Education, Universities and Research, 2012-ATE-0179 grant to EDS and PJ_RIC_FFABR_2017_161560 grant to AI.

Bibliographic references

Allen, J.I., Somerfield, P.J., Siddorn, J., 2002. Primary and bacterial production in the Mediterranean Sea: A modelling study. J Mar Syst 33–34, 473–495. doi:10.1016/S0924-7963(02)00072-6

Ausín, B., Flores, J.A., Sierro, F.J., Bárcena, M.A., Hernández-Almeida, I., Francés, G., Gutiérrez-Arnillas, E., Martrat, B., Grimalt, J.O., Cacho, I., 2015. Coccolithophore productivity and surface water dynamics in the Alboran Sea during the last 25kyr. Palaeogeogr Palaeoclimatol Palaeoecol 418, 126–140. doi:10.1016/j.palaeo.2014.11.011

Bahr, A., Kaboth, S., Jiménez-Espejo, F.J., Sierro, F.J., Voelker, A.H.L., Lourens, L., Röhl, U., Reichart, G.J., Escutia, C., Hernández-Molina, F.J., Pross, J., Friedrich, O., 2015. Persistent monsoonal forcing of Mediterranean Outflow Water dynamics during the late Pleistocene. Geology 43, 951–954.

Bazzicalupo, P., Maiorano, P., Girone, A., Marino, M., Combourieu-Nebout, N., Incarbona, A., 2018. High-frequency climate fluctuations over the last deglaciation in the Alboran Sea, Western Mediterranean: Evidence from calcareous plankton assemblages. Palaeogeogr Palaeoclimatol Palaeoecol. doi:10.1016/j.palaeo.2018.06.042

Beaufort, L., 1997. Insolation Cycles as a Major Control of Equatorial Indian Ocean Primary Production. Science 278, 1451–1454. doi:10.1126/science.278.5342.1451

Beaufort, L., de Garidel-Thoron, T., Mix, A.C., Pisias, N.G., 2001. ENSO-like forcing on oceanic primary production during the Late Pleistocene. Science 293, 2440–2444. doi:10.1126/science.293.5539.2440

Beaufort, L., Lancelot, Y., Camberlin, P., Cayre, O., Vincent, E., Bassinot, F., Labeyrie, L., 1997. Insolation Cycles as a Major Control of Equatorial Indian Ocean Primary Production. Science 278, 1451–1454.

Bond, G., Kromer, B., Beer, J., Muscheler, R., Evans, M.N., Showers, W., Hoffmann, S., Lotti-Bond, R., Hajdas, I., Bonani, G., 2001. Persistent solar influence on North Atlantic climate during the Holocene. Science 294, 2130–2136. doi:10.1126/science.1065680

Bond, G., Showers, W., Cheseby, M., Lotti, R., Almasi, P., DeMenocal, P., Priore, P., Cullen, H., Hajdas, I., Bonani, G., 1997. A pervasive millennial-scale cycle in North Atlantic Holocene

339 and glacial climates. Science 278, 1257–1266. doi:10.1126/science.278.5341.1257
340 Bown, P.R., Young, J.R., 1998. Techniques, in: Bown, P.R. (Ed.), Calcareous Nannofossil
341 Biostratigraphy. Chapman and Kluwer Academic, London, pp. 16–28.
342 Buccheri, G., Capretto, G., Di Donato, V., Esposito, P., Ferruzza, G., Pescatore, T., Russo Ermolli,
343 E., Senatore, M.R., Sprovieri, M., Bertoldo, M., Carella, D., Madonia, G., 2002. A high
344 resolution record of the last deglaciation in the southern Tyrrhenian sea: Environmental and
345 climatic evolution. Mar Geol 186, 447–470. doi:10.1016/S0025-3227(02)00270-0
346 Cacho, I., Grimalt, J.O., Canals, M., Sbaffi, L., Shackleton, N.J., Schönfeld, J., Zahn, R., 2001.
347 Variability of the western Mediterranean Sea surface temperature during the last 25,000 years
348 and its connection with the Northern Hemisphere climatic changes. Paleoceanography 16, 40–
349 52.
350 Casford, J.S.L., Rohling, E.J., Abu-Zied, R.H., Fontanier, C., Jorissen, F.J., Leng, M.J., Schmiedl,
351 G., Thomson, J., 2003. A dynamic concept for eastern Mediterranean circulation and
352 oxygenation during sapropel formation. Palaeogeogr Palaeoclimatol Palaeoecol 190, 103–119.
353 doi:10.1016/S0031-0182(02)00601-6
354 Castradori, D., 1993. Calcareous nannofossils and the origin of Eastern Mediterranean sapropel.
355 Paleoceanography 8, 459–471.
356 Cheng, H., Edwards, R.L., Sinha, A., Spötl, C., Yi, L., Chen, S., Kelly, M., Kathayat, G., Wang, X.,
357 Li, X., Kong, X., Wang, Y., Ning, Y., Zhang, H., 2016. The Asian monsoon over the past
358 640,000 years and ice age terminations. Nature 534, 640–646. doi:10.1038/nature18591
359 Cita, M.B., Beghi, C., Camerlenghi, A., Kastens, K.A., McCoy, F.W., Nosetto, A., Parisi, E.,
360 Scolari, F., Tomadin, L., 1984. Turbidites and megaturbidites from the Herodotus abyssal plain
361 (eastern Mediterranean) unrelated to seismic events. Mar Geol 55, 79–101.
362 doi:https://doi.org/10.1016/0025-3227(84)90134-8
363 Colmenero-Hidalgo, E., Flores, J.A., Sierro, F.J., Bárcena, M.Á., Löwemark, L., Schönfeld, J.,
364 Grimalt, J.O., 2004. Ocean surface water response to short-term climate changes revealed by
365 coccolithophores from the Gulf of Cadiz (NE Atlantic) and Alboran Sea (W Mediterranean).
366 Palaeogeogr Palaeoclimatol Palaeoecol 205, 317–336. doi:10.1016/j.palaeo.2003.12.014
367 Crudeli, D., Young, J.R., Erba, E., Geisen, M., Ziveri, P., de Lange, G.J., Slomp, C.P., 2006. Fossil
368 record of holococcoliths and selected hetero-holococcolith associations from the
369 Mediterranean (Holocene-late Pleistocene): Evaluation of carbonate diagenesis and
370 palaeoecological-palaeocenographic implications. Palaeogeogr Palaeoclimatol Palaeoecol 237,
371 191–212. doi:10.1016/j.palaeo.2005.11.022
372 D'Ortenzio, F., Ribera d'Alcalà, M., 2009. On the trophic regimes of the Mediterranean Sea: a

satellite analysis. Biogeosciences 6, 139–148. doi:10.5194/bg-6-139-2009

De Lange, G.J., Thomson, J., Reitz, A., Slomp, C.P., Principato, M.S., Erba, E., Corselli, C., 2008. Synchronous basin-wide formation and redox-controlled preservation of a Mediterranean sapropel 1. doi:10.1038/ngeo283

Di Stefano, A., Foresi, L.M., Incarbona, A., Sprovieri, M., Vallefuoco, M., Iorio, M., Pelosi, N., Di Stefano, E., Sangiorgi, P., Budillon, F., 2015. Mediterranean coccolith ecobiostratigraphy since the penultimate Glacial (the last 145,000years) and ecobioevent traceability. Mar Micropaleontol 115. doi:10.1016/j.marmicro.2014.12.002

~~Di Stefano, A., Foresi, L.M., Incarbona, A., Sprovieri, M., Vallefuoco, M., Iorio, M., Pelosi, N., Di Stefano, E., Sangiorgi, P., Budillon, F., 2015. Mediterranean coccolith ecobiostratigraphy since the penultimate Glacial (the last 145,000years) and ecobioevent traceability. Mar Micropaleontol 115, 24–38. doi:10.1016/j.marmicro.2014.12.002~~

Di Stefano, E., Incarbona, A., 2004. High-resolution palaeoenvironmental reconstruction of ODP Hole 963D (Sicily Channel) during the last deglaciation based on calcareous nannofossils. Mar Micropaleontol 52. doi:10.1016/j.marmicro.2004.04.009

Di Stefano, E., Incarbona, A., Bonomo, S., Pelosi, N., 2011. Coccolithophores in water samples and fossil assemblages in sedimentary archives of the Mediterranean Sea: A review, in: Martorino, L., Puopolo, K. (Eds.), New Oceanography Research Developments: Marine Chemistry, Ocean Floor Analyses and Marine Phytoplankton. Nova Science Publishers, Inc., pp. 127–162.

Dittert, N., Baumann, K.H., Bickert, T., Henrich, R., Huber, R., Kinkel, H., Meggers, H., 1999. Carbonate dissolution in the Deep-Sea: Methods, Quantification and Paleoceanographic Application, in: Fischer, G., Wefer, G. (Eds.), Use of Proxies in Paleoceanography: Examples from the South Atlantic. pp. 255–284.

Emeis, K.-C., Robertson, A.H.F., Richter, C., et al., 1996. Site 968. In Proceedings of the Ocean Drilling Program, Initial Reports 160, 289–333.

Flores, J.A., Bárcena, M.A., Sierro, F.J., 2000. Ocean-surface and wind dynamics in the Atlantic Ocean off Northwest Africa during the last 140 000 years. Palaeogeogr Palaeoclimatol Palaeoecol 161, 459–478. doi:10.1016/S0031-0182(00)00099-7

Flores, J.A., Sierro, F.J., Francés, G., Vazquez, A., Zamarreno, I., 1997. The last 100,000 years in the western Mediterranean: sea surface water and frontal dynamics as revealed by coccolithophores. Mar Micropaleontol 29, 351–366.

Frigola, J., Moreno, a., Cacho, I., Canals, M., Sierro, F.J., Flores, J. a., Grimalt, J.O., Hodell, D. a., Curtis, J.H., 2007. Holocene climate variability in the western Mediterranean region from a deepwater sediment record. Paleoceanography 22, 1–16. doi:10.1029/2006PA001307

Grant, K.M., Grimm, R., Mikolajewicz, U., Marino, G., Ziegler, M., Rohling, E.J., 2016. The timing of Mediterranean sapropel deposition relative to insolation, sea-level and African monsoon changes. Quat Sci Rev 140, 125–141. doi:10.1016/j.quascirev.2016.03.026

Grant, K.M., Rohling, E.J., Westerhold, T., Zabel, M., Heslop, D., Konijnendijk, T., Lourens, L., 2017. A 3 million year index for North African humidity/aridity and the implication of potential pan-African Humid periods. Quat Sci Rev 171, 100–118. doi:https://doi.org/10.1016/j.quascirev.2017.07.005

Grelaud, M., Marino, G., Ziveri, P., Rohling, E.J., 2012. Abrupt shoaling of the nutricline in response to massive freshwater flooding at the onset of the last interglacial sapropel event. Paleoceanography 27. doi:10.1029/2012PA002288

Grimm, R., Maier-Reimer, E., Mikolajewicz, U., Schmiedl, G., Müller-Navarra, K., Adloff, F., Grant, K.M., Ziegler, M., Lourens, L.J., Emeis, K.-C., 2015. Late glacial initiation of Holocene eastern Mediterranean sapropel formation. Nat Commun 6, 7099. doi:10.1038/ncomms8099

Hennekam, R., Donders, T.H., Zwiep, K., de Lange, G.J., 2015. Integral view of Holocene precipitation and vegetation changes in the Nile catchment area as inferred from its delta sediments. Quat Sci Rev 130, 189–199. doi:10.1016/j.quascirev.2015.05.031

Hilgen, F.J., 1991. Astronomical calibration of Gauss to Matuyama sapropels in the Mediterranean and implication for the Geomagnetic Polarity Time Scale. Earth Planet Sci Lett 104, 226–244. doi:10.1016/0012-821x(91)90206-w

Incarbona, A., Bonomo, S., Di Stefano, E., Zgozi, S., Essarbout, N., Talha, M., Tranchida, G., Bonanno, A., Patti, B., Placenti, F., Buscaino, G., Cuttitta, A., Basilone, G., Bahri, T., Massa, F., Censi, P., Mazzola, S., 2008a. Calcareous nannofossil surface sediment assemblages from the Sicily Channel (central Mediterranean Sea): Palaeoceanographic implications. Mar Micropaleontol 67. doi:10.1016/j.marmicro.2008.03.001

Incarbona, A., Di Stefano, E., Bonomo, S., 2009. Calcareous nannofossil biostratigraphy of the central Mediterranean Basin during the last 430,000 years. Stratigraphy 6, 33–44. doi:10.2307/1484315

Incarbona, A., Di Stefano, E., Patti, B., Pelosi, N., Bonomo, S., Mazzola, S., Sprovieri, R., Tranchida, G., Zgozi, S., Bonanno, A., 2008b. Holocene millennial-scale productivity variations in the Sicily Channel (Mediterranean Sea). Paleoceanography 23. doi:10.1029/2007PA001581

Incarbona, A., Martrat, B., Di Stefano, E., Grimalt, J.O., Pelosi, N., Patti, B., Tranchida, G., 2010a. Primary productivity variability on the Atlantic Iberian Margin over the last 70,000 years: Evidence from coccolithophores and fossil organic compounds. Paleoceanography 25, 1–15.

441 doi:10.1029/2008PA001709
442 Incarbona, A., Ziveri, P., Di Stefano, E., Lirer, F., Mortyn, G., Patti, B., Pelosi, N., Sprovieri, M.,
443 Tranchida, G., Vallefuoco, M., Albertazzi, S., Bellucci, L.G., Bonanno, A., Bonomo, S., Censi,
444 P., Ferraro, L., Giuliani, S., Mazzola, S., Sprovieri, R., 2010b. The Impact of the Little Ice Age
445 on Coccolithophores in the Central Mediterranea Sea. Clim Past 6, 795–805. doi:10.5194/cp-6-
446 795-2010
447 Incarbona, A., Ziveri, P., Sabatino, N., Manta, D.S., Sprovieri, M., 2011. Conflicting
448 coccolithophore and geochemical evidence for productivity levels in the Eastern
449 Mediterranean sapropel S1. Mar Micropaleontol 81. doi:10.1016/j.marmicro.2011.09.003
450 Jilbert, T., Reichart, G.-J., Mason, P., de Lange, G.J., 2010. Short-time-scale variability in
451 ventilation and export productivity during the formation of Mediterranean sapropel S1.
452 Paleoceanography 25. doi:10.1029/2010PA001955
453 Jordan, R.W., Cros, L., Young, J.R., 2004. A revised classification scheme for living haptophytes.
454 Micropaleontology 50, 55–79. doi:10.2113/50.Suppl_1.55
455 Jorissen, F.J., 1999. Benthic foraminiferal successions across Late Quaternary Mediterranean
456 sapropels. Mar Geol 153, 91–101.
457 Josey, S.A., Somot, S., Tsimplis, M., 2011. Impacts of atmospheric modes of variability on
458 Mediterranean Sea surface heat exchange. J Geophys Res Ocean 116, 1–15.
459 doi:10.1029/2010JC006685
460 Kemp, A.E.S., Pearce, R.B., Koizumi, I., Pike, J., Rance, S.J., 1999. The role of mat-forming
461 diatoms in the formation of Mediterranean sapropels. Nature 398, 57.
462 Kleijne, A., 1991. Holococcolithophorids from the Indian-Ocean, Red-Sea, Mediterranean-Sea and
463 North-Atlantic Ocean. Mar Micropaleontol 17, 1–76. doi:Doi 10.1016/0377-8398(91)90023-Y
464 Klein, P., Coste, B., 1984. Effects of wind-stress variability on nutrient transport into the mixed
465 layer. Deep Sea Res Part A Oceanogr Res Pap 31, 21–37. doi:https://doi.org/10.1016/0198-
466 0149(84)90070-0
467 Knappertsbusch, M., 1993. Geographic distribution of living and Holocene coccolithophores in the
468 Mediterranean Sea. Mar Micropaleontol. doi:10.1016/0377-8398(93)90016-Q
469 Konijnendijk, T.Y.M., Ziegler, M., Lourens, L., 2014. Chronological constraints on Pleistocene
470 sapropel depositions from high-resolution geochemical records of ODP Sites 967 and 968,
471 Newsletters on Stratigraphy. doi:10.1127/0078-0421/2014/0047
472 Krom, M.D., Emeis, K.C., Van Cappellen, P., 2010. Why is the Eastern Mediterranean phosphorus
473 limited? Prog Oceanogr 85, 236–244. doi:10.1016/j.pocean.2010.03.003
474 Krom, M.D., Kress, N., Brenner, S., Gordon, L.I., 1991. Phosphorus Limitation of Primary

475 Productivity in the Eastern Mediterranean-Sea. Limnol Oceanogr 36, 424–432.
476 Leonhardt, A., Toledo, F.A.L., Coimbra, J.C., 2015. The Mid-Brunhes Event in the Southwestern
477 Atlantic Ocean: Coccolithophore assemblages during the MIS 11-9. Rev Bras Paleontol 18,
478 343–354. doi:10.4072/rbp.2015.3.01
479 López-Otálvaro, G.-E., Flores, J.A., Sierro, F.J., Cacho, I., Grimalt, J.-O., Michel, E., Cortijo, E.,
480 Labeyrie, L., 2009. Late Pleistocene palaeoproductivity patterns during the last climatic cycle
481 in the Guyana Basin as revealed by calcareous nannoplankton. eEarth 4, 1–13. doi:10.5194/ee-
482 4-1-2009
483 Lourens, L.J., Antonarakou, A., Hilgen, F.J., Van Hoof, a. a. M., Vergnaud-Grazzini, C.,
484 Zachariasse, W.J., 1997. Evaluation of the Plio-Pleistocene astronomical timescale.
485 Paleoceanography 12, 527. doi:10.1029/97PA00321
486 Lourens, L.J., Wehausen, R., Brumsack, H.J., 2001. Geological constraints on tidal dissipation and
487 dynamical ellipticity of the Earth over the past three million years. Nature 409, 1029.
488 Malanotte-Rizzoli, P., Artale, V., Borzelli-Eusebi, G.L., Brenner, S., Crise, A., Gacic, M., Kress,
489 N., Marullo, S., Ribera D'Alcalà, M., Sofianos, S., Tanhua, T., Theocharis, A., Alvarez, M.,
490 Ashkenazy, Y., Bergamasco, A., Cardin, V., Carniel, S., Civitarese, G., D'Ortenzio, F., Font,
491 J., Garcia-Ladona, E., Garcia-Lafuente, J.M., Gogou, A., Gregoire, M., Hainbucher, D.,
492 Kontoyannis, H., Kovacevic, V., Kraskapoulou, E., Kroskos, G., Incarbona, A., Mazzocchi,
493 M.G., Orlic, M., Ozsoy, E., Pascual, A., Poulain, P.M., Roether, W., Rubino, A., Schroeder,
494 K., Siokou-Frangou, J., Souvermezoglou, E., Sprovieri, M., Tintoré, J., Triantafyllou, G.,
495 2014. Physical forcing and physical/biochemical variability of the Mediterranean Sea: A
496 review of unresolved issues and directions for future research. Ocean Sci 10, 281–322.
497 doi:10.5194/os-10-281-2014
498 Marino, G., Rohling, E.J., Sangiorgi, F., Hayes, A., Casford, J.L., Lotter, A.F., Kucera, M.,
499 Brinkhuis, H., 2009. Early and middle Holocene in the Aegean Sea: interplay between high
500 and low latitude climate variability. Quat Sci Rev 28, 3246–3262.
501 doi:10.1016/j.quascirev.2009.08.011
502 McIntyre, A., Molfino, B., 1996. Forcing of Atlantic Equatorial and Subpolar Millennial Cycles by
503 Precession. Science. doi:10.1126/science.274.5294.1867
504 Meier, K.J.S., 2004. Different nutrient sources forcing increased productivity during eastern
505 Mediterranean S1 sapropel formation as reflected by calcareous dinoflagellate cysts.
506 Paleoceanography 19, 1–12. doi:10.1029/2003PA000895
507 Mercone, D., Thomson, J., Abu-Zied, R.H., Croudace, I.W., Rohling, E.J., 2001. High-resolution
508 geochemical and micropalaeontological profiling of the most recent eastern Mediterranean

509 sapropel. Mar Geol 177, 25–44. doi:10.1016/S0025-3227(01)00122-0
510 Molfino, B., McIntyre, A., 1990a. Precessional forcing of nutricline dynamics in the equatorial
511 atlantic. Science 249, 766–769. doi:10.1126/science.249.4970.766
512 Molfino, B., McIntyre, A., 1990b. Nutricline variation in the equatorial Atlantic coincident with the
513 Younger Dryas. Paleoceanography. doi:10.1029/PA005i006p00997
514 Negri, A., Capotondi, L., Keller, J., 1999. Calcareous nannofossils, planktonic foraminifera and
515 oxygen isotopes in the late Quaternary sapropels of the Ionian Sea. Mar Geol 157, 89–103.
516 doi:10.1016/S0025-3227(98)00135-2
517 Negri, A., Giunta, S., 2001. Calcareous nannofossil paleoecology in the sapropel S1 of the Eastern
518 Ionian sea: Paleoceanographic implications. Palaeogeogr Palaeoclimatol Palaeoecol 169, 101–
519 112. doi:10.1016/S0031-0182(01)00219-X
520 Oviedo, A., Ziveri, P., Álvarez, M., Tanhua, T., 2015. Is coccolithophore distribution in the
521 Mediterranean Sea related to seawater carbonate chemistry? Ocean Sci 11, 13–32.
522 doi:10.5194/os-11-13-2015
523 Pinardi, N., Masetti, E., 2000. Variability of the large scale general circulation of the Mediterranean
524 Sea from observations and modelling: A review. Palaeogeogr Palaeoclimatol Palaeoecol 158,
525 153–174. doi:10.1016/S0031-0182(00)00048-1
526 POEM group, 1992. General-Circulation of the Eastern Mediterranean. Earth-Science Rev 32, 285–
527 309.
528 Poulos, S.E., Drakopoulos, P.G., Collins, M.B., 1997. Seasonal variability in sea surface
529 oceanographic conditions in the Aegean Sea (Eastern Mediterranean): an overview. J Mar Syst
530 13, 225–244. doi:https://doi.org/10.1016/S0924-7963(96)00113-3
531 Rohling, E.J., Cane, T.R., Cooke, S., Sprovieri, M., Bouloubassi, I., Emeis, K.C., Schiebel, R.,
532 Kroon, D., Jorissen, F.J., Lorre, a., Kemp, a. E.S., 2002. African monsoon variability during
533 the previous interglacial maximum. Earth Planet Sci Lett 202, 61–75. doi:10.1016/S0012-
534 821X(02)00775-6
535 Rohling, E.J., Gieskes, W.W., 1989. Late Quaternary changes in Mediterranean intermediate water
536 density and formaton rate. Paleoceanography 4, 531–545.
537 Rohling, E.J., Jorissen, F.J., De stigter, H.C., 1997. 200 Year interruption of Holocene sapropel
538 formation in the Adriatic Sea. J Micropalaeontology. doi:10.1144/jm.16.2.97
539 Rohling, E.J., Marino, G., Grant, K.M., 2015. Mediterranean climate and oceanography, and the
540 periodic development of anoxic events (sapropels). Earth-Science Rev.
541 doi:10.1016/j.earscirev.2015.01.008
542 Rossignol-Strick, M., 1985. Mediterranean Quaternary sapropels, an immediate response of the

543 African monsoon to variation of insolation. Palaeogeogr Palaeoclimatol Palaeoecol 49, 237–
544 263. doi:https://doi.org/10.1016/0031-0182(85)90056-2
545 Rossignol-Strick, M., Nesteroff, W., Olive, P., Vergnaud-Grazzini, C., 1982. After the deluge:
546 Mediterranean stagnation and sapropel formation. Nature 295, 105.
547 Rutten, a., De Lange, G.J., Ziveri, P., Thomson, J., Van Santvoort, P.J.M., Colley, S., Corselli, C.,
548 2000. Recent terrestrial and carbonate fluxes in the pelagic eastern Mediterranean; a
549 comparison between sediment trap and surface sediment. Palaeogeogr Palaeoclimatol
550 Palaeoecol 158, 197–213. doi:10.1016/S0031-0182(00)00050-X
551 Schmiedl, G., Mitschele, A., Beck, S., Emeis, K., Hemleben, C., Schulz, H., Sperling, M., Weldeab,
552 S., 2003. Benthic foraminiferal record of ecosystem variability in the eastern Mediterranean
553 Sea during times of sapropel S 5 and S 6 deposition. Palaeogeogr, Palaeoclim Palaeoecol 190,
554 139–164.
555 Schönfeld, J., Zahn, R., 2000. Late Glacial to Holocene history of the Mediterranean outflow.
556 Evidence from benthic foraminiferal assemblages and stable isotopes at the Portuguese margin.
557 Palaeogeogr Palaeoclimatol Palaeoecol 159, 85–111. doi:10.1016/S0031-0182(00)00035-3
558 Thomson, J., Crudeli, D., De Lange, G.J., Slomp, C.P., Erba, E., Corselli, C., Calvert, S.E., 2004.
559 Florisphaera profunda and the origin and diagenesis of carbonate phases in eastern
560 Mediterranean sapropel units. Paleoceanography 19, 1–19. doi:10.1029/2003PA000976
561 Triantaphyllou, M. V, 2014. Coccolithophore assemblages during the Holocene Climatic Optimum
562 in the NE Mediterranean (Aegean and northern Levantine Seas, Greece): Paleoceanographic
563 and paleoclimatic implications. Quat Int. doi:10.1016/j.quaint.2014.01.033
564 Triantaphyllou, M. V, Antonarakou, A., Dimiza, M.D., Anagnostou, C., 2010. Calcareous
565 nannofossil and planktonic foraminiferal distributional patterns during deposition of sapropels
566 S6, S5 and S1 in the Libyan Sea (Eastern Mediterranean). Geo-Marine Lett 30, 1–13.
567 doi:10.1007/s00367-009-0145-7
568 Triantaphyllou, M. V, Antonarakou, A., Kouli, K., Dimiza, M.D., Kontakiotis, G., Papanikolaou,
569 M.D., Ziveri, P., Mortyn, P.G., Lianou, V., Lykousis, V., Dermitzakis, M.D., 2009a. Late
570 Glacial-Holocene ecostratigraphy of the south-eastern Aegean Sea, based on plankton and
571 pollen assemblages. Geo-Marine Lett 29, 249–267. doi:10.1007/s00367-009-0139-5
572 Triantaphyllou, M. V, Ziveri, P., Gogou, A., Marino, G., Lykousis, V., Bouloubassi, I., Emeis,
573 K.C., Kouli, K., Dimiza, M.D., Rosell-Melé, A., Papanikolaou, M., Katsouras, G., Nunez, N.,
574 2009b. Late Glacial-Holocene climate variability at the south-eastern margin of the Aegean
575 Sea. Mar Geol 266, 182–197. doi:10.1016/j.margeo.2009.08.005
576 Voelker, A.H.L., Lebreiro, S.M., Schönfeld, J., Cacho, I., Erlenkeuser, H., Abrantes, F., 2006.

577 Mediterranean outflow strengthening during northern hemisphere coolings: A salt source for
578 the glacial Atlantic? Earth Planet Sci Lett 245, 39–55. doi:10.1016/j.epsl.2006.03.014
579 Wehausen, R., Brumsack, H., 2000. Chemical cycles in Pliocene sapropel-bearing and sapropel-
580 barren eastern Mediterranean sediments. Palaeogeogr Palaeoclimatol Palaeoecol 158, 325–
581 352.
582 Weldeab, S., Menke, V., Schmiedl, G., 2014. The pace of East African monsson evolution during
583 the Holocene. Geophys Res Lett 41, 1724–1731. doi:10.1002/2014GL059361.Received
584 Young, J.R., 1994. Functions of coccoliths, in: Winter, A., Siesser, W.G. (Eds.), Coccolithopphores.
585 Cambridge Univ. Press, Cambridge, pp. 63–82.
586 Young, J.R., Geisen, M., Cros, L., Kleijne, A., Sprengel, C., Probert, I., Østergaard, J., 2003. A
587 guide to extant coccolithophore taxonomy. J Nannoplankt Res 125.
588 Zahn, R., Sarnthein, M., Erlenkeuser, H., 1987. Benthic isotope evidence for changes of the
589 Mediterranean outflow during the Late Quaternary. Paleoceanography 2, 543–559.
590 doi:10.1029/PA002i006p00543
591
592
593 Captions
594 Figure 1: Bathymetric map of the eastern Mediterranean Sea and core location. The black arrow
595 indicates the path of MAW. EMDW: Eastern Mediterranean Deep Water. Grey arrows indicate the
596 EMDW outflow into the deep eastern Mediterranean Sea. The dashed grey arrow shows the
597 location of Shikmona and Mers a-Matruh gyres system. The blue and red circles respectively
598 indicate the location of ODP Site 968 and 967 (present study; Emeis et al., 1996; Konijnendijk et
599 al., 2014; Grant et al., 2017). The green circle indicates the location of core SL112 (Weldeab et al.,
600 2014).
601
602 Figure 2: High-resolution photograph of sapropel S1 and colour lightness at ODP Hole 968C
603 (Emeis et al., 1996).
604
605 Figure 3: Downcore variations of selected calcareous nannofossil species at ODP Hole 968C,
606 plotted *versus* depth (centimetres composite depth - cmcd). From the left, it is shown the relative
607 abundance of *E. huxleyi*, *F. profunda*, holococcoliths and small *Gephyrocapsa*. Black arrows in the
608 *E. huxleyi* distribution pattern show the high-frequency variability within sapropel S1. The relative
609 abundance of calcareous nannofossil reworked specimens is also shown. The vertical grey band
610 indicates the extent of sapropel S1. The coloured vertical bars show the 95 % confidence level error

associated to the counting for each taxon.

Figure 4: Downcore variations of selected calcareous nannofossil species at ODP Hole 968C, plotted *versus* depth (cmcd). From the left, it is shown the relative abundance of *S. pulchra*, *U. sibogae*, *Umbellosphaera* spp., *D. tubifera* and *S. histrica*. The vertical grey band indicates the extent of sapropel S1. The coloured vertical bars show the 95 % confidence level error associated to the counting for each taxon.

Figure 5: Downcore variations of selected calcareous nannofossil groups at ODP Hole 968C, plotted *versus* depth (cmcd). From the left, it is shown the relative abundance of Placoliths, Miscellaneous, UPZ, LPZ and holococcoliths. Black arrows in the Placoliths distribution pattern show the high-frequency variability within sapropel S1. The vertical grey band indicates the extent of sapropel S1. The coloured vertical bars show the 95 % confidence level error associated to the counting for each group.

Figure 6: Downcore variations of calcareous nannofossils at ODP Hole 968C (present study) and geochemical and geophysical records from the eastern Mediterranean, plotted *versus* age (ka). (A): calcareous nannofossil N ratio at ODP 968C (present study), used as a proxy for nutricline depth. Black arrows show the high-frequency variability within sapropel S1. (B): Monsoon Index, calculated as the difference between the Tropic of Cancer and the Equator insolation (Rossignol-Strick et al., 1982, 1985). (C): Ba/Ca ratio calculated at SL112 core, as a proxy for Nile River runoff (Weldeab et al., 2014). (D): Composite record of $\delta^{18}O$ speleothem values from Chinese caves, as a proxy for Asian Monsoon activity (Cheng et al., 2016). (E): Holococcoliths at ODP 968C (present study), used as a proxy for seafloor and/or pore water calcite preservation. (F): Colour lightness at ODP 968C (Emeis et al., 1996). (G): Wet/dry index, calculated by elemental proxies at ODP Site 967 (Grant et al., 2017). (H): CEX index at ODP 968C (present study), used as a proxy for coccolith dissolution. (I): Calcareous nannofossil reworked specimens at ODP 968C (present study). (J): Ti/Al ratio at the ODP 967/968 composite section, used as a proxy for aeolian dust deposition (Konijnendijk et al., 2014).

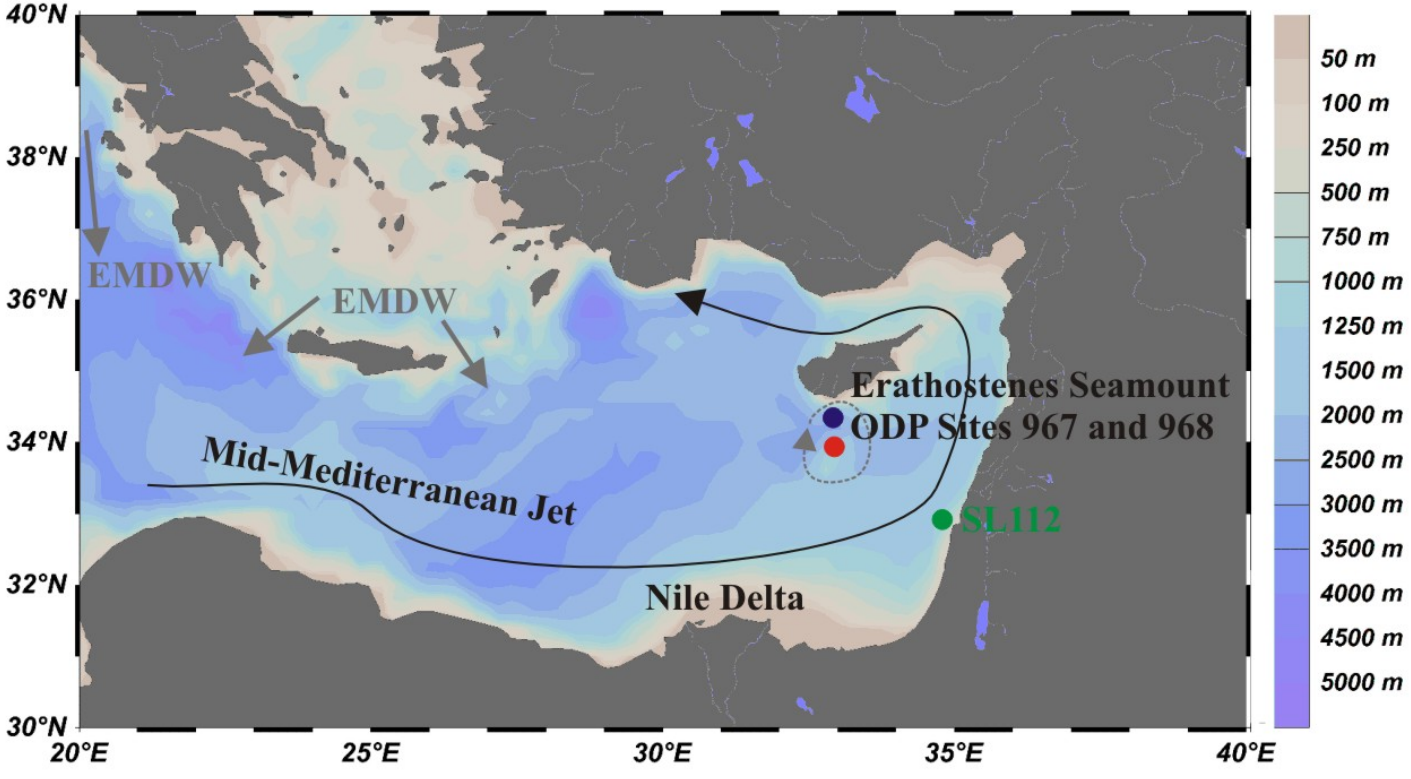
40°N
38°N
36°N
34°N
32°N
30°N
20°E
25°E
30°E
35°E
40°E
EMDW
EMDW
Erathostenes Seamount
ODP Sites 967 and 968
Mid-Mediterranean Jet
SL112
Nile Delta
50 m
100 m
250 m
500 m
750 m
1000 m
1250 m
1500 m
2000 m
2500 m
3000 m
3500 m
4000 m
4500 m
5000 m

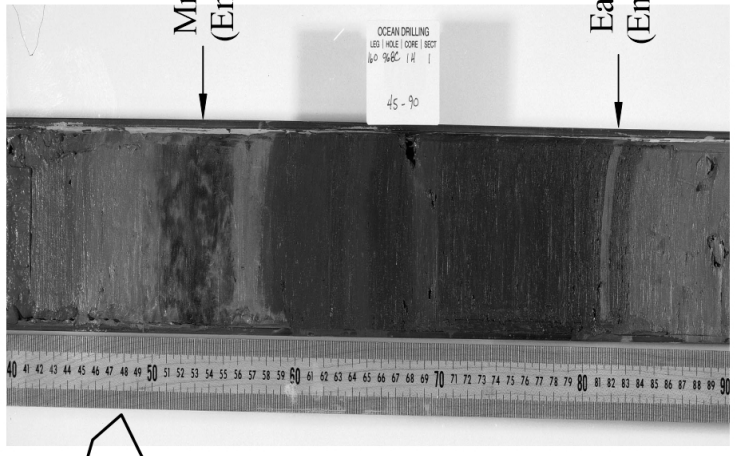

Mn-enriched layer (Emeis et al., 1996)

Early interruption (Emeis et al., 1996)

Photograph of sapropel S1 in Hole 968C (Emeis et al., 1996)

Colour lightness (L*) ODP 968 (Emeis et al., 1996)

56
52
48
44
40
36

0.2
0.4
0.6
0.8
1
1.2

Depth (mbsf)

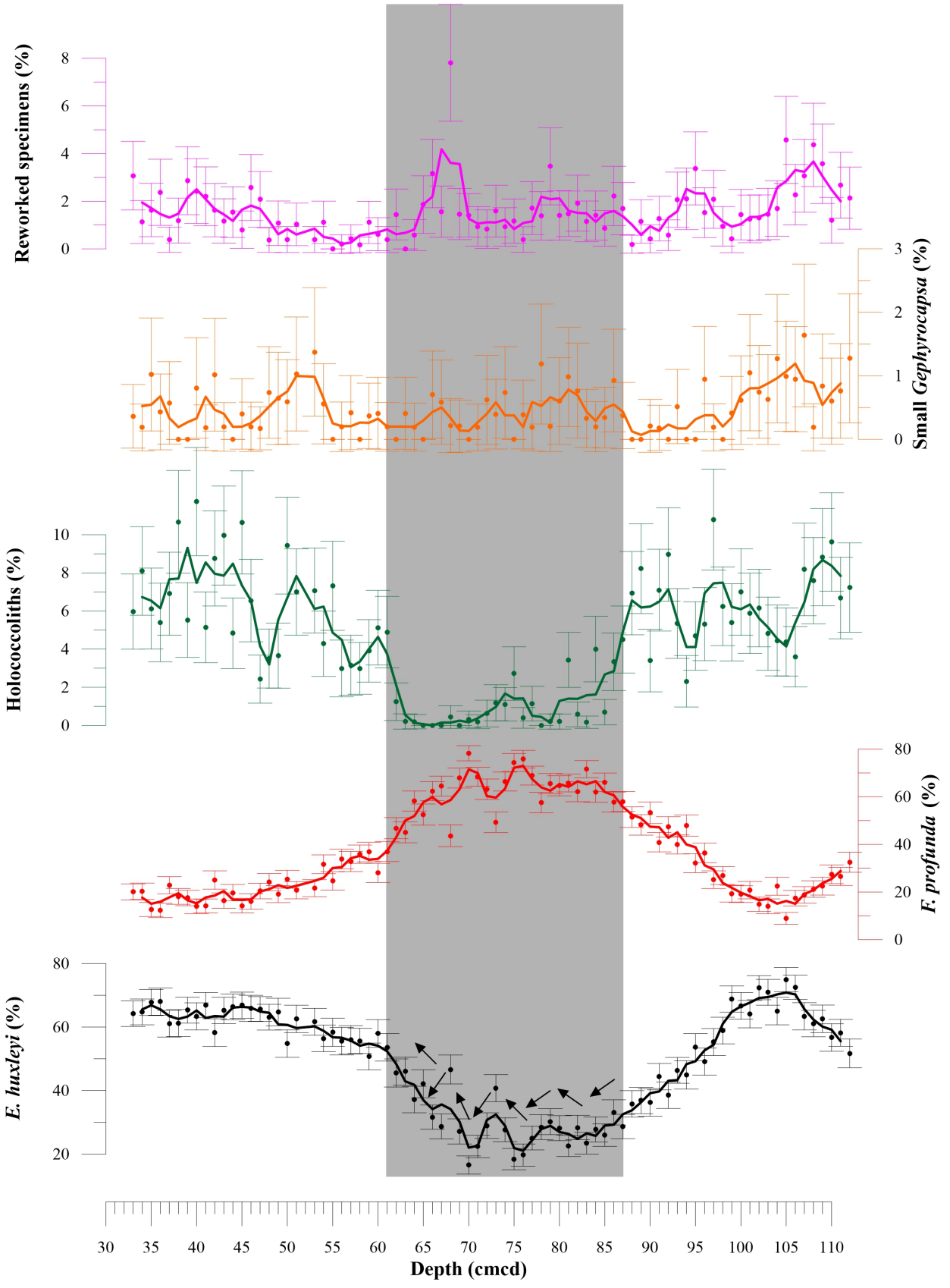
Reworked specimens (%)
0
2
4
6
8
Small Gephyrocapsa (%)
0
1
2
3
Holococcoliths (%)
0
2
4
6
8
10
F. profunda (%)
0
20
40
60
80
E. huxleyi (%)
20
40
60
80
30
35
40
45
50
55
60
65
70
75
80
85
90
95
100
105
110
Depth (cmcd)

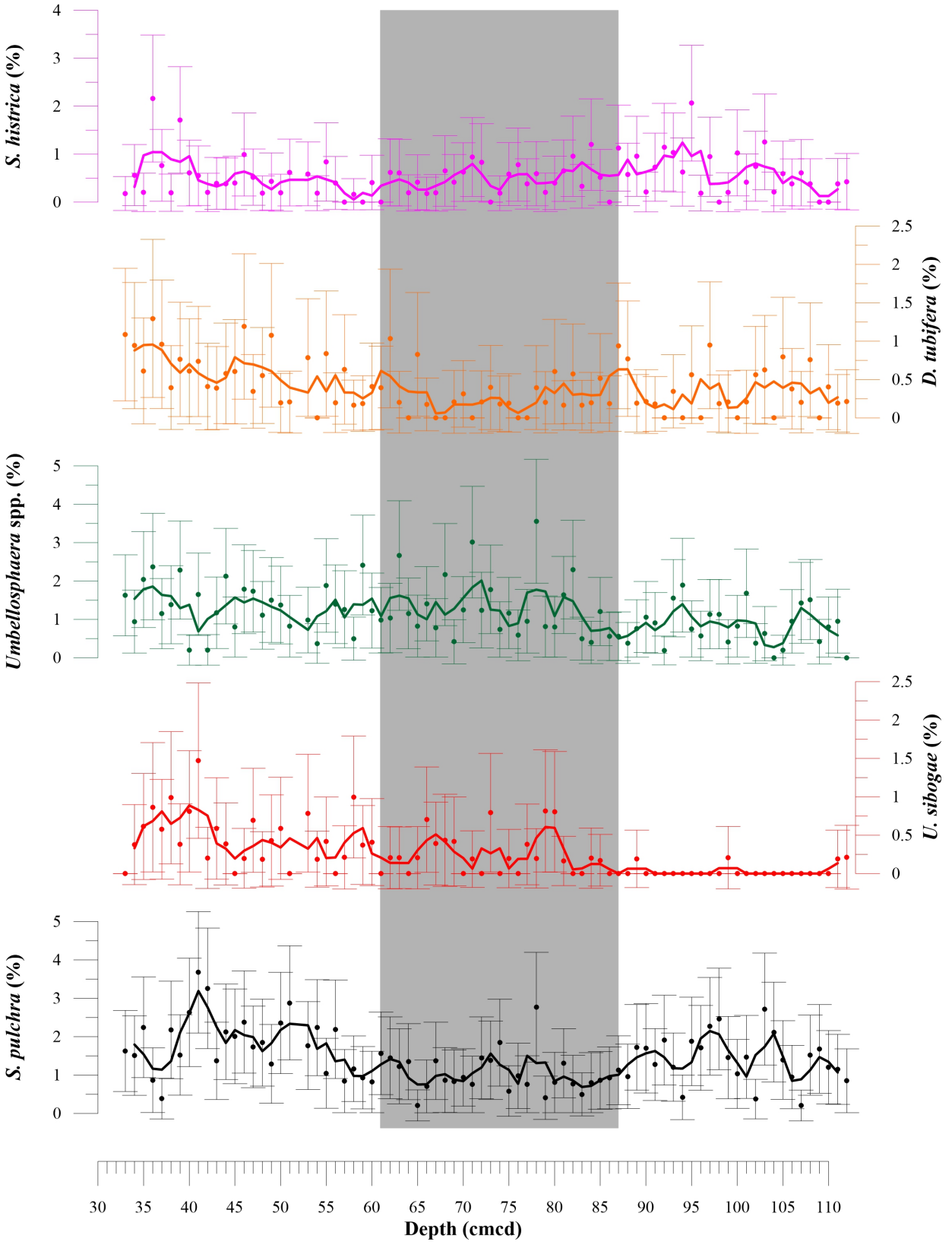
S. histrica (%)
D. tubifera (%)
Umbellosphaera spp. (%)
U. sibogae (%)
S. pulchra (%)
Depth (cmcd)

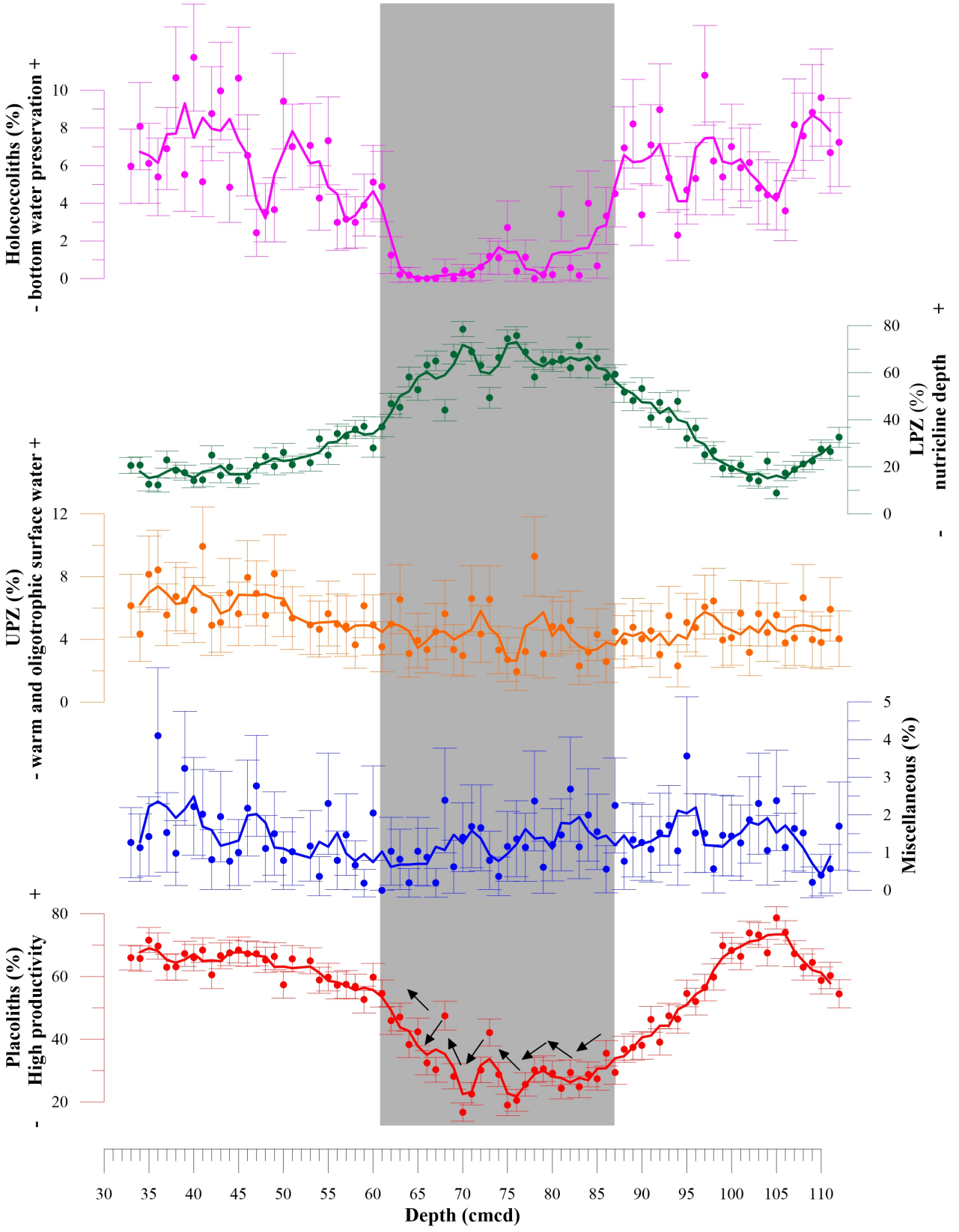
Holococcoliths (%)
- bottom water preservation +
0
2
4
6
8
10
LPZ (%)
- nutricline depth +
0
20
40
60
80
UPZ (%)
- warm and oligotrophic surface water +
0
4
8
12
Miscellaneous (%)
0
1
2
3
4
5
Placoliths (%)
- High productivity +
20
40
60
80
30
35
40
45
50
55
60
65
70
75
80
85
90
95
100
105
110
Depth (cmcd)

N ratio ODP 968
+ Nutricline depth -
Ba/Ca µmol/mol SL112
(Weldeab et al., 2014)
- Nile River discharge +
Holococcoliths ODP 968
+ Coccolith preservation -
wet/dry index ODP 967
(Grant et al., 2017)
- Wetness +
Reworked specimens (%) ODP 968
CEX ODP 968
Colour lightness (L*) ODP 968
(Emeis et al., 1996)
- Dark colour +
Composite δ18O speleothems (‰)
(Cheng et al., 2016)
- Asian monsoon activity +
Monsoon index
Ti/Al ODP 967/968
(Konijnendijk et al., 2014)
- Aeolian dust +
(A)
(B)
(C)
(D)
(E)
(F)
(G)
(H)
(I)
(J)
Age (ka)